J. Fluid Mech. (1992), *vol.* 245, *pp.* 47–68

Görtler vortex formation at the inner cylinder in Taylor–Couette flow

By T. WEI[1], E. M. KLINE[1], S. H.-K. LEE[1] AND S. WOODRUFF[2]

[1]Department of Mechanical and Aerospace Engineering, Rutgers University, Piscataway, NJ 08855-0909, USA

[2]Engineering Division, Brown University, Providence, RI 02912, USA

(Received 31 December 1991 and in revised form 5 June 1992)

The evolution of small counter-rotating circumferential vortices in Taylor–Couette flow was examined using the laser induced fluorescence and alumina particle flow visualization techniques. The objective of the study was to critically evaluate the hypothesis of Barcilon *et al.* (1979) and Barcilon & Brindley (1984) that Görtler vortices form close to the cylinder walls at moderately high Taylor numbers. Three radius ratios spanning an order of magnitude, $0.084 \leqslant R_{in}/R_{out} \leqslant 0.877$, were examined over a Taylor number range of $3 \times 10^4 \leqslant Ta \leqslant 3 \times 10^8$. Still-photograph sequences taken from video records of the LIF experiments are presented showing vortex pairs close to the inner cylinder wall at Taylor numbers an order of magnitude smaller than those reported by Barcilon and co-workers. Measurements of the core-to-core separation between counter-rotating vortices were made in order to estimate the wavenumber of the instability. These measurements agree remarkably well with the theoretical analysis of Barcilon and co-workers particularly for the small- and medium-gap experiments. The present measurements indicate that there is a $-\frac{1}{3}$ power law relationship between the Görtler wavelength and Taylor number. This is consistent with the work of Barcilon & Brindley (1984). However, the present study indicates that the Görtler vortices first form at the inner cylinder wall, and that a full theoretical treatment must include inner-wall effects.

1. Introduction

In the late 1970s, Swinney & Gollub conducted their now famous studies in Taylor–Couette flows showing that transition to turbulence is better described as a chaotic process rather than as an infinite succession of hydrodynamic instabilities. A detailed description of their work may be found in Fenstermacher, Swinney & Gollub (1979). At the same time, Barcilon *et al.* (1979) were conducting very similar experiments but focusing on coherent structures in the moderate to high Taylor number range. They formulated an hypothesis that at high Taylor numbers, boundary layers form close to the cylinder walls which subsequently become unstable to Görtler-type instabilities. They presented photographs showing 'herringbone shaped streaks' which they argued was evidence of Görtler vortices at the outer cylinder wall. Later, Barcilon & Brindley (1984) developed an analysis providing a theoretical basis for their hypothesis. To date, however, there are no flow visualization studies which clearly show the formation of streamwise counter-rotating vortices forming close to the cylinder walls.

The objective of this investigation was to critically evaluate the Barcilon *et al.* (1979), Barcilon & Brindley (1984) hypothesis. Specifically, it will be shown that

counter-rotating vortices do in fact appear close to the cylinder walls at high Taylor numbers. The significant results from this work, in which a larger range of Taylor numbers and gap widths were examined, were that the counter-rotating vortices appeared first at the inner cylinder wall, these vortices occurred at Taylor numbers an order of magnitude lower than those predicted in the earlier studies.

1.1. *Definitions*

Before proceeding, it is necessary to note that there are a number of definitions of Taylor number, Ta, commonly in use. In this paper, Ta will be defined as

$$Ta = R_{\text{in}}\Omega^2 d^3/\nu^2 = (U_{\text{in}}^2 d^2/\nu^2)(d/R_{\text{in}}) = (Re_d^2)(d/R_{\text{in}}), \tag{1}$$

where R_{in}, R_{out} are the inner and outer cylinder radii, respectively, Ω the inner cylinder angular velocity, $d = R_{\text{out}} - R_{\text{in}}$ the gap width, ν the kinematic viscosity (in this case of water), $U_{\text{in}} = R_{\text{in}}\Omega$ the circumferential speed of the inner cylinder surface, and $Re_d = U_{\text{in}} d/\nu$.

1.2. *A brief literature review*

Flow between concentric cylinders has proven to be a remarkably rich problem in fluid dynamics. Beginning with the early work of Taylor (1923), a myriad of complex and interesting phenomena have been observed and examined. The body of literature is correspondingly expansive. Part of the fascination with the Taylor–Couette problem is the fact that such a simple flow geometry can produce such complexities. Much of the work involves studies of instabilities which manifest themselves at Taylor numbers slightly higher than the critical value for the onset of Taylor vortices. Examples include papers by Iooss (1986), Benjamin & Mullin (1982), and Cliffe & Mullin (1985), amongst many others. The problem of interest here, however, is the transition to turbulence which takes place at higher Taylor numbers than the works just cited.

Fenstermacher *et al.* (1979) critically evaluated Landau's postulate that turbulence occurs through an infinite succession of hydrodynamic instabilities. They used laser-Doppler anemometry to obtain spectra of the time-varying circumferential velocity in a Taylor–Couette flow with large aspect ratio. They also used reflective particles to visually observe the flow. For simplicity, they considered only the case of stationary outer cylinder and rotating inner cylinder. In their flow visualization studies, they observed an evolution to turbulence with increasing Taylor number. This evolution began with the formation of laminar axisymmetric toroidal vortices, followed by wavy toroidal vortices, and subsequently followed by the appearance of turbulent axisymmetric toroids. They observed that during this evolution the measured velocity spectra showed the presence of only two discrete frequencies before the flow exhibited chaotic behaviour. They argued that according to Landau's postulate, the spectra should contain an increasing number of discrete-frequency spikes with increasing Taylor number. The fact that only two such peaks were observed before the spectra became broadband was strong evidence that the Landau postulate was not applicable. Because Fenstermacher *et al.* (1979) were more interested in transition as a dynamical system, they did not investigate the eddy structure of the flow in detail.

Barcilon *et al.* (1979) conducted a very similar experiment which did concentrate on the coherent structures associated with transition. They examined three different test fluids in a narrow-gap experiment where the inner cylinder was rotated and the outer cylinder was stationary. Results included still photographs which looked very

similar to those of Fenstermacher *et al.* (1979). For Taylor numbers greater than 400 times the critical onset Taylor number, they observed a 'herring-bone pattern of streaks' whose appearance seemed to coincide with the presence of high-frequency fluctuations in the hot-film signals. Using insightful physical arguments, they concluded that these observations could be explained by the formation of Görtler-type vortices close to the cylinder walls.

To provide a firm theoretical foundation for their hypothesis, Barcilon & Brindley (1984) formulated a mathematical model of the small-gap Taylor–Couette flow at high Taylor number. They postulated the existence of two instabilities. Taylor and Görtler, with highly separated lengthscales. In that way, two independent stability problems could be treated and coupled using the method of matched asymptotic expansions. The justification for the large separation of scales was predicated on the argument that thin boundary layers form adjacent to the cylinder walls. This premise was supported with both experimental data and physical arguments. Barcilon & Brindley (1984) computed the wavelength of the Görtler vortices as a function of Taylor number and compared it to estimates made by examining their photographs. They concluded that Görtler vortices are responsible for the 'herring-bone' patterns observed in Barcilon *et al* (1979).

Smith & Townsend (1982) and shortly thereafter, Townsend (1984) extended the analysis to even higher Taylor number to study the transition to turbulence. In both papers, single $\times$-probe and multiple-sensor hot-wire anemometry were used to examine the fine-scale structure in Taylor–Couette flow for Taylor numbers up to 4×10^9. In order to obtain accurate mean statistics, a very low axial velocity was created in the gap to advect the flow structures past the stationary probes. The data obtained in these studies supported the idea of small-scale structure generation in the boundary layers close to the cylinder walls. Townsend (1984) argued that at moderately large Taylor numbers the velocity fluctuations associated with the small scales were Görtler vortices. However, in the very large Taylor number range, the near-wall turbulent structure was believed to exhibit characteristics similar to plane turbulent boundary layer flows.

1.3. *On the formation of Görtler vortices at the inner cylinder wall*

At the outset, it would be worthwhile to establish that Görtler vortices can form close to the inner cylinder wall of the Taylor–Couette experiment. In the original Görtler (1954) analysis, the boundary-layer flow over a stationary concave wall was shown to be unstable. A simple physical explanation of the Görtler mechanism is that there is a balance between the pressure gradient normal to the wall and the radial momentum flux of the flow, the centrifugal forces. For a concave wall, the circumferential velocity increases with decreasing radius (going away from the wall). This results in a radial pressure distribution where the pressure is highest at the wall. This pressure gradient serves to 'turn' the fluid around the concave bend. If the flow speed is increased, or the radius of curvature decreased, the pressure at the wall will not be sufficiently large to 'turn' the flow and Görtler vortices are generated.

In the case of a fixed convex wall, with fluid moving around it, the radial inertia of the fluid and the radial pressure forces both act in the direction away from the wall. Görtler vortices do not occur in this case. In Taylor–Couette flow, however, the inner cylinder is a moving convex wall. The circumferential velocity decreases with increasing radius (again going away from the wall). In this case, there is again a balance between the pressure gradient and the inertia of the flow. For a moving convex wall, the pressure gradient acts to 'turn' the flow around the convex bend.

So again, when the circumferential velocity is increased or the radius of curvature is decreased, the radial inertia of the flow will exceed the pressure forces and Görtler vortices will be generated.

For Görtler vortices, the characteristic non-dimensional parameter should contain information about the boundary-layer thickness, the radius of curvature of the wall, and the free-stream velocity. Görtler (1954) defined this non-dimensional number as

$$G = (U_\infty^2 \delta^2/\nu^2)\,\delta/R, \tag{2}$$

where U_∞, δ, and R are the free-stream velocity, boundary-layer thickness, and radius of curvature, respectively. Note that in a Taylor–Couette flow, there will be a different Görtler number for each cylinder; an appropriate 'free-steam' velocity needs to be defined for each cylinder wall.

1.4. *Objectives*

At this juncture, there have been no flow visualization studies done which clearly show the formation of small-scale counter-rotating vortices close to either the inner or outer cylinder walls. The limitation can be principally attributed to inadequacies in the flow visualization techniques used. That is, alumina particles or dyes illuminated from a diffuse light source will not provide the radial cross-sections of the flow needed to see the rotation of circumferentially oriented vortices.

It has been well established that these small structures play a significant role in the transition from laminar Taylor vortices to turbulence. However, that role is not well understood. In the Taylor–Couette experiment, inner- and outer-cylinder wall boundary layers exist which are separated by and strongly influenced by the presence of the large Taylor vortices. This makes for an extremely complex flow. Consequently, direct visual studies of the gap are essential to a clear understanding of the dynamics and kinematics of the transition process.

In this investigation, laser-induced-fluorescence flow visualization techniques were used to examine the fluid motions in the (r, z)-plane (i.e. orthogonal to the circumferential direction). The objectives of this study were: to provide conclusive visual evidence of small-scale counter-rotating vortex pairs (Görtler vortices) close to the inner cylinder wall; and to critically evaluate the assumptions of Barcilon & Brindley (1984) in the light of the present results.

2. Apparatus

A Taylor–Couette experiment consisting of a circular inner cylinder rotating concentrically inside a stationary outer cylinder was constructed for this investigation. The working fluid was water. Two flow visualization techniques including laser-induced fluorescence (LIF) and alumina particles were used to examine the flow. A brief description of the cylinder assembly appears in the following paragraphs; the reader is referred to Lee (1990) for greater detail. The flow visualization apparatus is described in §3. A drawing of the apparatus appears in figure 1.

The outer cylinder was made from 153.35 cm long section of clear Plexiglas pipe with an inner diameter of 30.28 cm. Three different-diameter inner cylinders were used so that a range of gap sizes could be examined. The smallest of these cylinders was a 2.54 cm diameter brass shaft which also served as the drive shaft for the two larger inner cylinders. The brass shaft was 198 cm long and is shown in figure 1 extending through the entire assembly. Two removable larger inner cylinders were

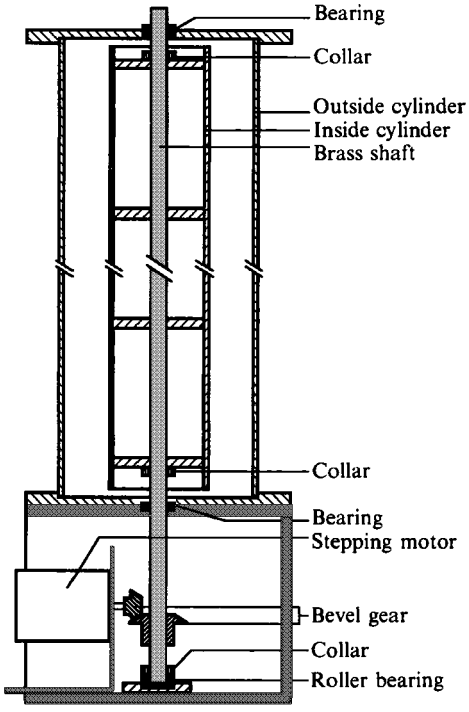

FIGURE 1. Schematic drawing of the side-view assembly of the Taylor–Couette experiment, including the stepping motor, brass drive shaft, medium inner cylinder, and outer cylinder.

made from 152.40 cm lengths of Plexiglas pipe. The outer diameters measured 15.04 and 26.57 cm for the medium and large inner cylinders, respectively. The corresponding aspect ratios (length:gap width) were 82:1, 20:1, and 11:1 for the 1.85, 7.62 and 13.87 cm gaps, respectively.

A number of steps were taken to make the cylinders circular and to precisely centre the inner cylinder(s) inside the outer cylinder. First, spacer assemblies were constructed for the two larger inner cylinders to centre them on the brass drive shaft. Each assembly consisted of four precision machined circular plates with centred clearance holes that were cemented inside the inner cylinder (normal to the cylinder axis). Second, the inner cylinder assemblies were turned on a lathe to machine the outer diameter to machine tolerances.

Finally, the end plates for the experiment were precision machined to ensure that the brass shaft was centred inside the outer cylinder and that tolerances on the inner diameter of the outer cylinder were maintained. Restraining plates were also placed around the outer cylinder to ensure a circular outer cylinder. The logic was that if the ends of the cylinder were forced into a circular restraint, then the rest of the cylinder would be forced to follow shape, at least to some degree. This was checked by measuring the outer diameter of the outer cylinder at the mid-height after the experiment was assembled. At the mid-height, the mean outer diameter of the outer cylinder was 30.76 cm, and the maximum deviation from the mean was 0.03 cm. The mean wall thickness was 0.48 cm with a maximum deviation of 0.018 cm.

The outer diameters of the two larger inner cylinders were also measured after being machined. The outer diameters were measured at 30.48 cm intervals along the entire length of the cylinders and at the mid-lengths. At each axial location, diameter measurements were made at 30° intervals around the cylinders' circumference. For

both inner cylinders, the maximum deviation in these measurements was less than 0.013 cm.

The final component of the apparatus was the drive system. The brass shaft was driven by a 25000 step-per-revolution microstepping motor and driver. Bevel gears with a 2:1 gear ratio were used to couple the motor output shaft to the brass inner cylinder drive shaft, as shown in figure 1. This resulted in the inner cylinders turning at a rate of one cylinder revolution per 50000 motor steps. A square-wave generator was used as the input to the motor controller.

The motor controller produced a synchronization pulse after every motor step. This pulse was monitored along with the sweep-generator input signal during each experimental run using a dual-trace oscilloscope. When the motor speed varied measurably, the run was repeated.

3. Experimental methods

3.1. *Flow visualization techniques*

Two different flow visualization techniques were used in this study. The primary visualization technique was LIF. However, to tie this work to previous studies, standard-time-exposure photography of alumina particles was also used. The LIF studies were done using an Innova 70-4 argon ion laser operating in all lines mode. The laser beam was aimed radially through the centre of the cylinders and spread into a vertical laser sheet by a 2.54 cm focal length cylindrical lens, illuminating the flow in the (r, z)-plane. This is shown in figure 2. The thickness of the sheet was ~ 0.2 cm. The advantage of this viewing orientation was that it was possible to see flow patterns close to the inner cylinder wall.

The fluid was marked with fluorescein dye injected upstream of the laser sheet. For the small- and medium-diameter inner cylinders (i.e. the large- and medium-gap cases), dye was injected using a syringe and a long stainless steel tube of 0.15 cm outer diameter inserted between the cylinders through a hole in the top end plate. The most effective method of marking the flow close to the inner cylinder was to slowly bleed dye right onto the surface of the inner cylinders and subsequently remove the injection tube. For the Taylor numbers examined, dye remained at the inner cylinder surface several minutes after the injection tube was withdrawn. Near-wall vortices would entrain dyed fluid away from the inner cylinder wall, making the vortices visible.

For the small-gap experiments, dye was slowly injected through a vertical row of 0.10 cm diameter holes drilled in the side of the outer cylinder. The row was 30.48 cm long and centred about the mid-height of the outer cylinder. This alternative injection method was used because the small gap was too small to easily manoeuvre the stainless steel tube, and the rotation speeds of the inner cylinder were high enough that the dye was quickly washed off the inner cylinder surface.

To establish that the near-wall eddies were not caused by the dye injection methods, a cloud of dye was placed into the gap before spinning the inner cylinder. The inner cylinder was then rotated at the speed corresponding to the desired Taylor number. While the quality of the visualization was not very high, it was good enough to observe the flow close to the inner cylinder wall. This test was run for a number of Taylor numbers for each gap size. In every case, the flow patterns observed using the dye cloud were identical to those seen using the dye injection techniques described in the previous paragraphs. It was concluded that the injection techniques did not adversely affect the flow.

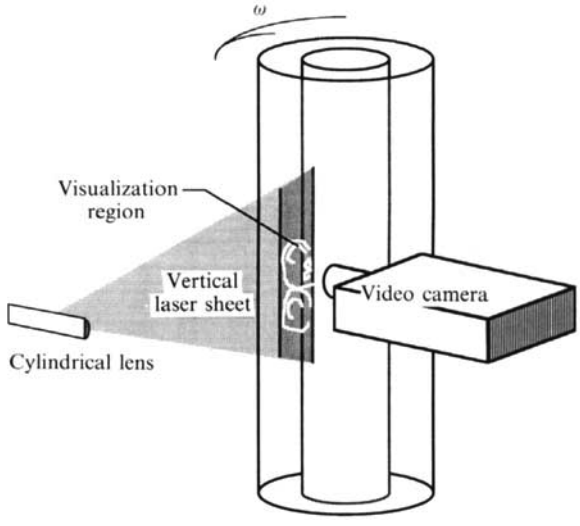

FIGURE 2. Oblique-view drawing showing the LIF visualization apparatus and orientation.

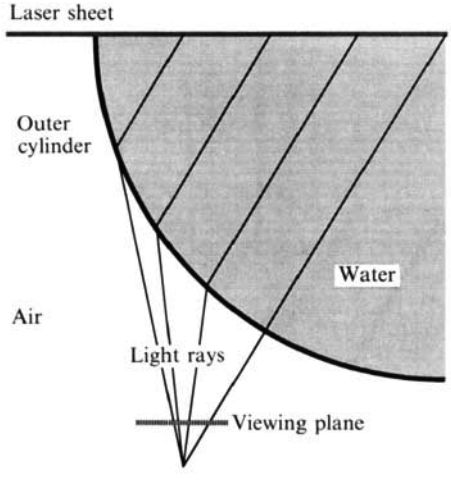

FIGURE 3. Top-view schematic showing the refraction effects associated with a curved wall.

Gap width, d (cm)	R_{in}/R_{out}	Aspect ratio (length/gap)	Ta_{crit}	Ta-range	Ta/Ta_{crit}-range
1.85	0.88	82	1500	30×10^3–30×10^5	20–2000
7.62	0.50	20	4700	30×10^5–137×10^6	638–29150
13.87	0.084	11	290000	10×10^6–300×10^6	34–1035

TABLE 1. Parameter range for the Taylor–Couette investigation. A range of Taylor numbers was examined for each of three different gap sizes. The critical Taylor number is defined in the text.

Visual records of the LIF experiments were made using a Sony professional quality $\frac{3}{4}$ in. video system. This included a 3CCD colour camera, video recorder, and frame code generator. The $\frac{3}{4}$ in. system was equipped with variable slow motion and frame-by-frame playback.

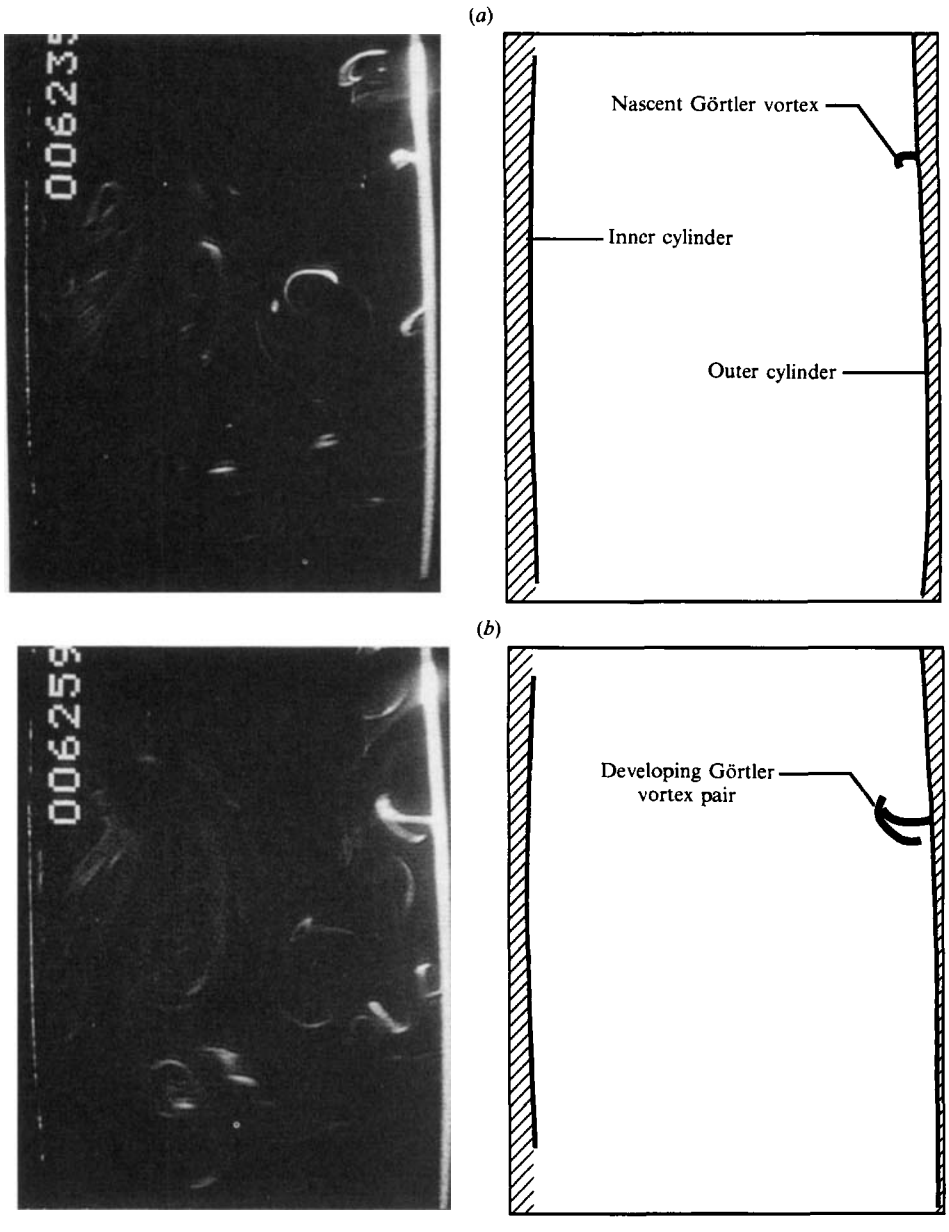

FIGURE 4(a, b). For caption see page 57.

The video camera was positioned to view the entire gap. The orientations of the laser sheet and the video camera are shown in figure 2. Because of the curvature of the cylinders, there were non-uniform refraction effects in the radial direction; objects close to the inner cylinder appeared larger than objects close to the outer cylinder. This effect is illustrated schematically in figure 3 which shows initially parallel light rays emanating from various radial locations in the cylinder and passing through a 'viewing plane' representing the camera lens. As long as the camera was far away from the cylinders, refraction effects in the axial direction were minimal.

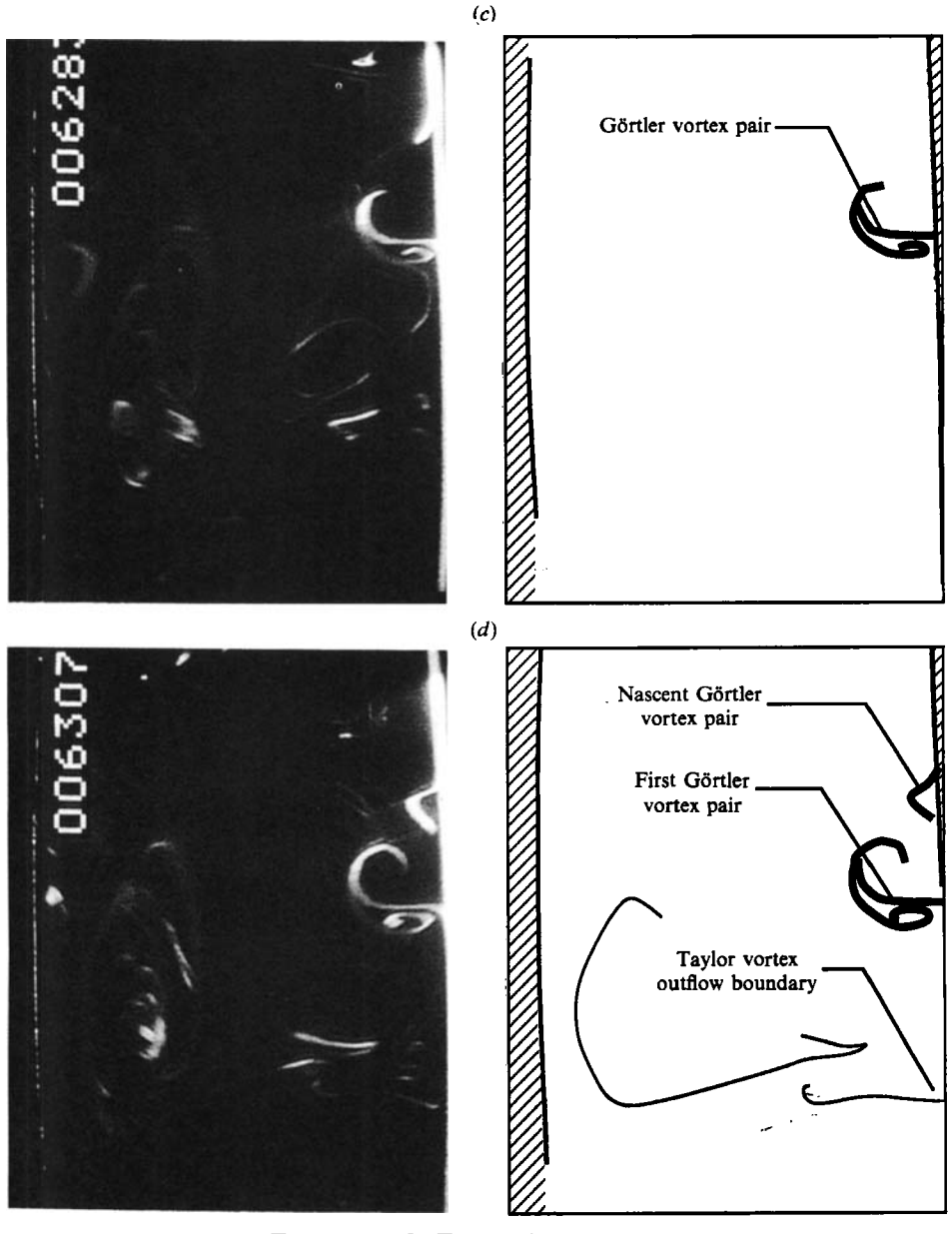

FIGURE 4(*c*, *d*). For caption see page 57.

3.2. *Quantitative analysis: measurement of the Görtler wavelength*

To facilitate subsequent theoretical analysis, estimates of the characteristic wavelength of the Görtler instabilities near the inner cylinder were needed. Results of this analysis are presented in §4.2. It will first be necessary to provide a description of the analysis. Note that a numerical stability analysis has recently been completed to complement the present study: the results from that study will appear in a separate paper by Woodruff & Wei.

It was decided that the core-to-core separation distance between two counter-rotating vortices in a Görtler vortex pair should be measured in order to estimate the most unstable Görtler wavelength. The most unstable wavelength could be obtained

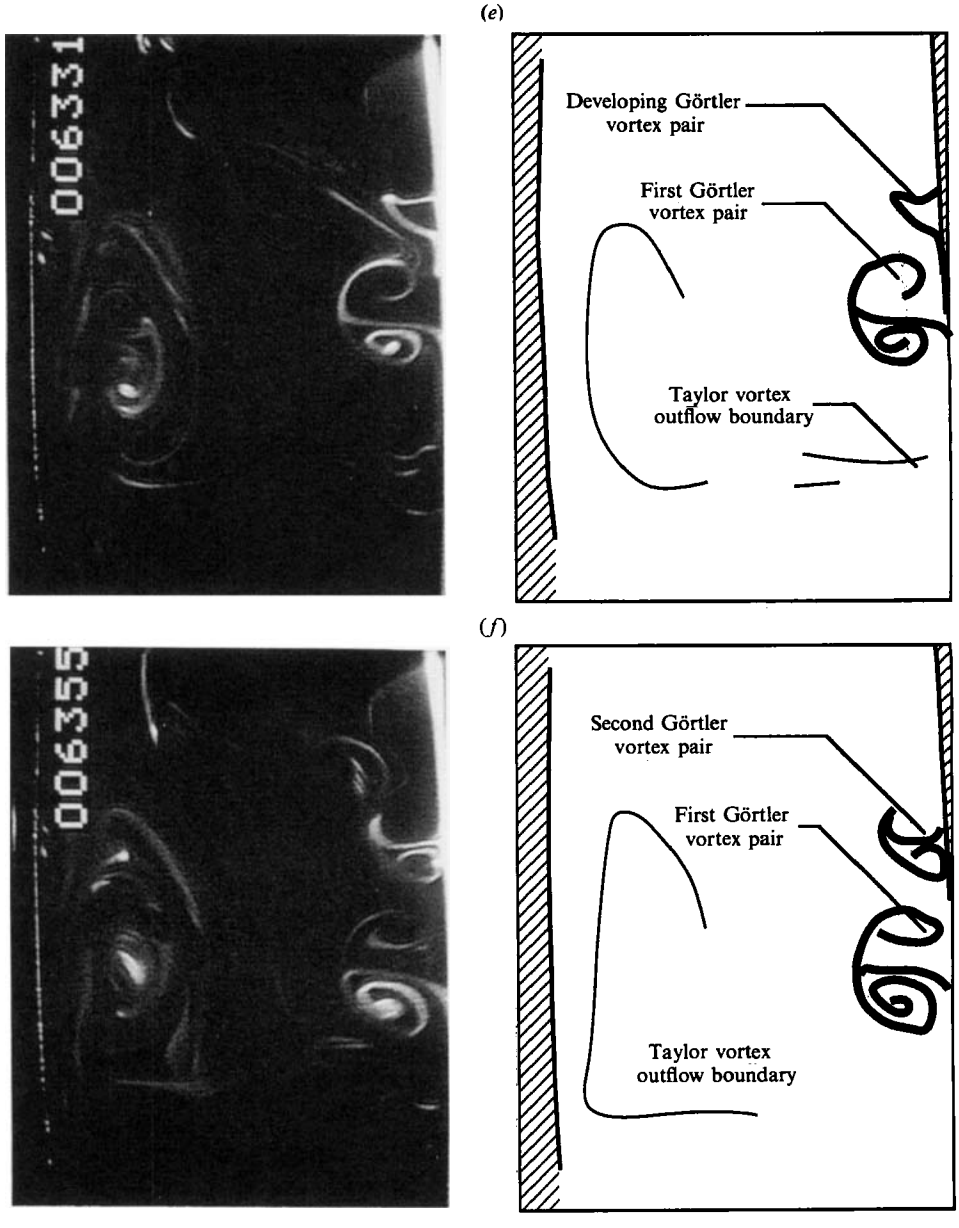

FIGURE 4(*e*,*f*). For caption see page 57.

by multiplying the core-to-core measurement by two. This choice was made primarily because single Görtler vortex pairs were observed far more frequently than multiple pairs. The small samples of multiple pairs virtually eliminated the possibility of measuring the distance between vortices of like rotation in adjacent Görtler vortex pairs.

To improve the most unstable wavelength approximation, core-to-core measurements were made as soon as the pair was visible. Measurements were done with the aid of the reverse slow-motion playback feature of the video recorder. For a given Taylor number, the video was played until a counter-rotating vortex pair was seen. The tape was then reversed in slow motion playback until the vortex pair could just

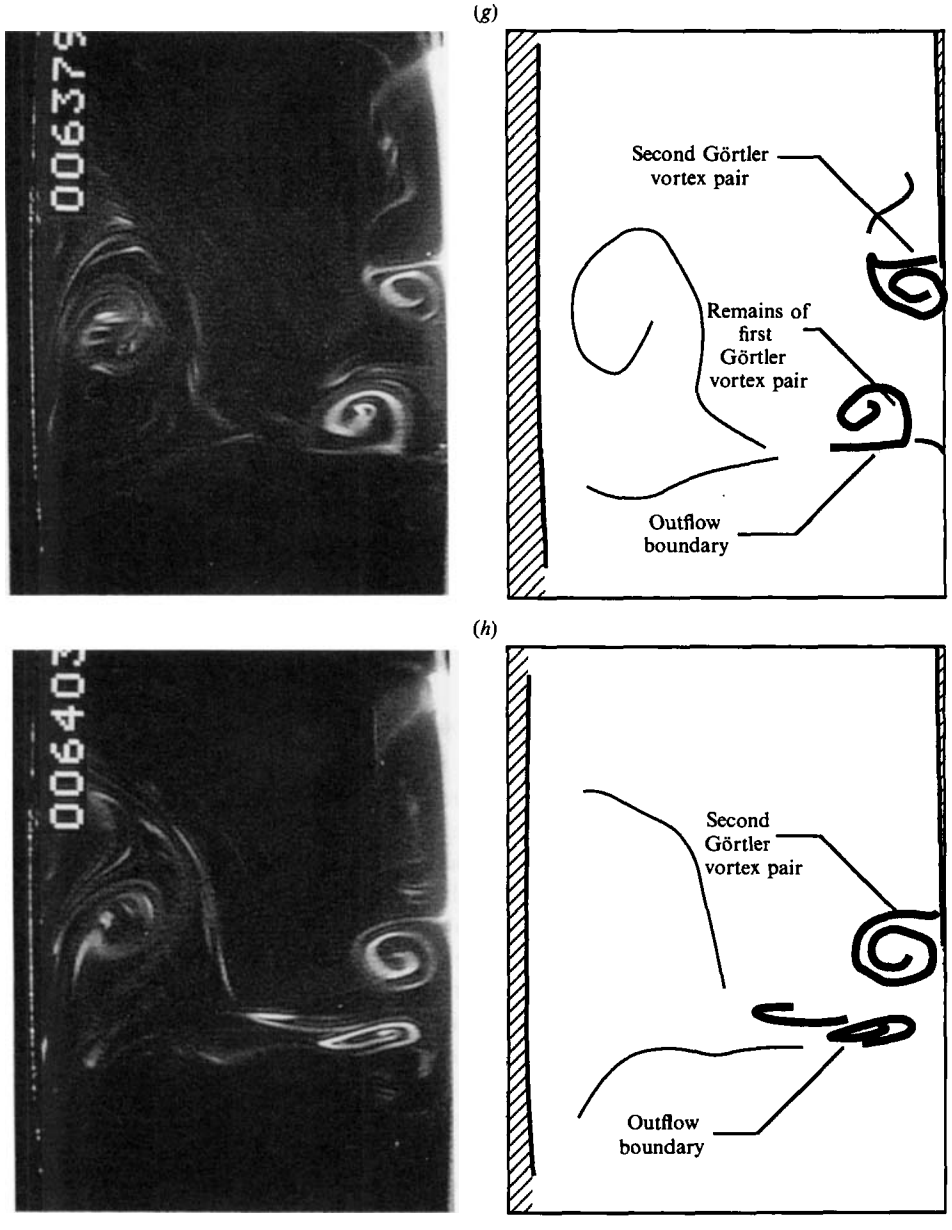

FIGURE 4 (*a–h*). Sequence of still photographs showing the formations and growth of Görtler vortex pairs at the inner cylinder wall. Pictures were taken from a video record of the medium gap at $Ta/Ta_{crit} = 2128$. The stationary outer cylinder appears on the left of the photographs and the rotating inner cylinder appears on the right. The mean circumferential flow is out of the page. Time elapse between successive photographs is 0.8 s. Line drawings of the photographs, highlighting important features in the flow appear to the right of each photograph.

barely be identified. The video frame was then frozen and the core-to-core measurement was made. The location of a vortex core was generally identifiable as a small spot near the centre of the vortex which contained no dye. In certain instances, the exact location of the cores was difficult to determine and the approximate centre was used.

In order to account for the uncertainties in the core-to-core measurements, a

number of independent measurements were made for each Taylor number. Wherever possible, a sample size of twenty to twenty-five different vortex pairs were examined for a given Taylor number and gap size. Exceptions included the low Taylor number cases for all three gap sizes and the high Taylor number cases for the small gap, where the number of vortex pairs observed was relatively small, and only five to ten different vortex pairs were measured for each case.

3.3. *Experimental conditions*

A wide range of Reynolds numbers were examined in this investigation using three different gap sizes, 1.85, 7.62 and 13.87 cm. For each gap size, a range of Taylor numbers spanning over an order of magnitude was studied; the range of parameters is shown in table 1. The overall range of Taylor numbers covered in this study was $3 \times 10^4 \leqslant Ta \leqslant 3 \times 10^8$.

The critical Taylor number, Ta_{crit}, in table 1 refers to the lowest value of Ta at which Taylor vortices first appear. The values of Ta_{crit} for the larger two gaps, presented in table 1, were obtained by interpolating the results of Sparrow, Munro & Jonsson (1964), and Walowit, Tsao & DiPrima (1964). The value for the small-gap case was based on the observation that Taylor cells were seen in the experiment at Taylor numbers slightly lower than the theoretical limit.

4. Results

4.1. *Visual observations*

In this section, still photographs of the flow visualizations are presented. The first set of photographs, figures 4–8, were taken from video records of the LIF studies. A number of time-exposure photographs of alumina particle visualization studies are also included in figure 9. The viewer orientation for all of the LIF photographs is the same. To assist in the interpretation of the visual images, computer assisted line tracings of the photographs have been included where necessary. The stationary outer cylinder appears on the left-hand side of the photographs, and is usually visible as a vertical white line. The rotating inner cylinder appears on the right-hand side of the photographs and can also be distinguished as a vertical white line. The rotation of the inner cylinder is always such that the mean circumferential flow is out of the page toward the viewer. Note that the cylinder walls appear curved in some of the photographs. This effect was caused by lens distortion of the Graflex camera used to make the photographs.

Figure 4 is a sequence of eight still photographs taken from an LIF video record of a medium-gap run at a Taylor number of 1×10^7; this corresponds to $Ta/Ta_{\text{crit}} = 2128$. The elapsed time between successive photographs is 0.8 s. The total duration of the sequence in figure 4 is 5.6 s. This corresponds to half a cylinder revolution. In this sequence, each photograph is filled primarily by a single Taylor cell which is rotating in a clockwise direction; this can be most easily seen in the video tapes. An outflow boundary appears near the bottom of the pictures, particularly in figure 4(*e–g*).

In figure 4(*a*), there is a bright spot along the inner cylinder wall located approximately a quarter of the way down the photograph. This is labelled in the corresponding line drawing. Observation of the video tape in real time indicates that this spot evolves into a counter-rotating vortex pair.

A short time later, figure 4(*b*), one can see that the spot has become 'tau' shaped as dye on the inner cylinder wall is lifted away from the wall into this flow structure.

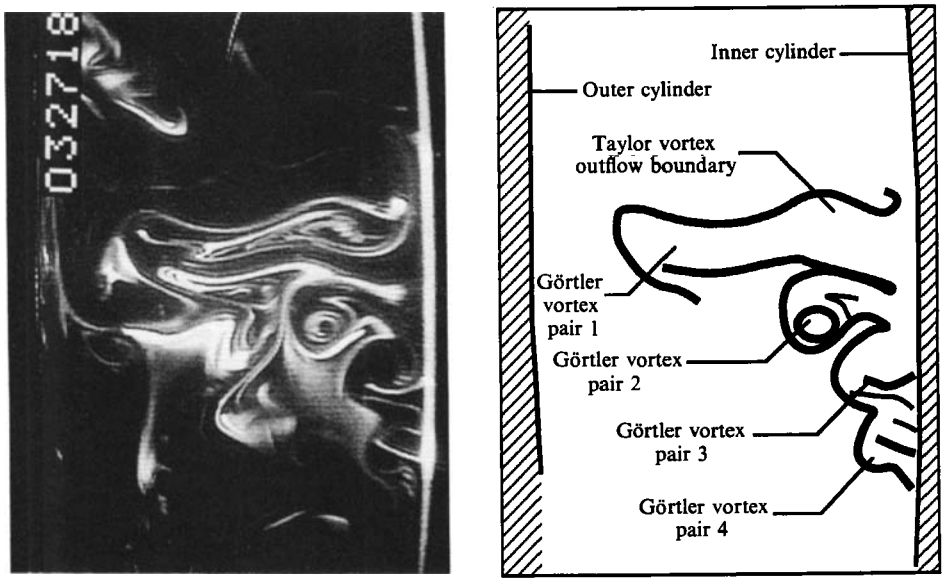

FIGURE 5. Single still photograph and line drawings showing four simultaneously occurring Görtler vortex pairs. The photograph was taken from a medium-gap video record at $Ta/Ta_{crit} = 6383$. The orientation of the flow is the same as in figure 4.

In figure 4(*c*), the classic mushroom shape of a counter-rotating vortex pair is readily evident. Owing to the motion of the large Taylor cell, the vortex pair is being advected downward in the picture.

In figure 4(*d*), dye continues to be entrained into the vortex pair. It is possible to see the first evidence of a second vortex pair. This appears as a kink of dye immediately above the first vortex pair. The motion of the Taylor vortex continues to move the near-wall fluid downward. In figure 4(*e*), the first vortex pair is located at the centre right of the picture. The existence of the second vortex pair is clearly discernible in figure 4(*f*). In that frame, there are two mushroom shaped structures close to the inner cylinder wall.

The rotation of the Taylor cell continues to move the near-wall vortex pairs toward the outflow boundary. In figure 4(*g*), the outflow boundary appears approximately three-quarters of the way down the photograph. In this frame, the first near-wall vortex pair was advected into the outflow boundary. One can see vestiges of the first vortex pair at the outflow boundary. The second vortex pair can be seen approaching the outflow boundary.

Once in the outflow boundary, the near-all vortices are deformed by the jet flow away from the wall. Depending on how energetic the near-wall vortices were, in the higher Taylor number flows, it was possible to track some of them all the way out to the outer cylinder. In the final photograph, figure 4(*h*), the first vortex pair has been significantly deformed by the outflow boundary. The only remaining evidence of the first pair is the elongated spiral shape at the base of the outflow boundary. The second vortex pair very close to the outflow boundary at this point is about to experience a similar fate.

Figure 5 is a single still photograph taken from a medium-gap LIF run at $Ta/Ta_{crit} = 6383$, showing part of a Taylor cell filling the bottom three-quarters of the photograph. The sense of rotation of the Taylor cell is counter-clockwise. Four counter-rotating vortex pairs appear in this photograph. The smallest appears at the

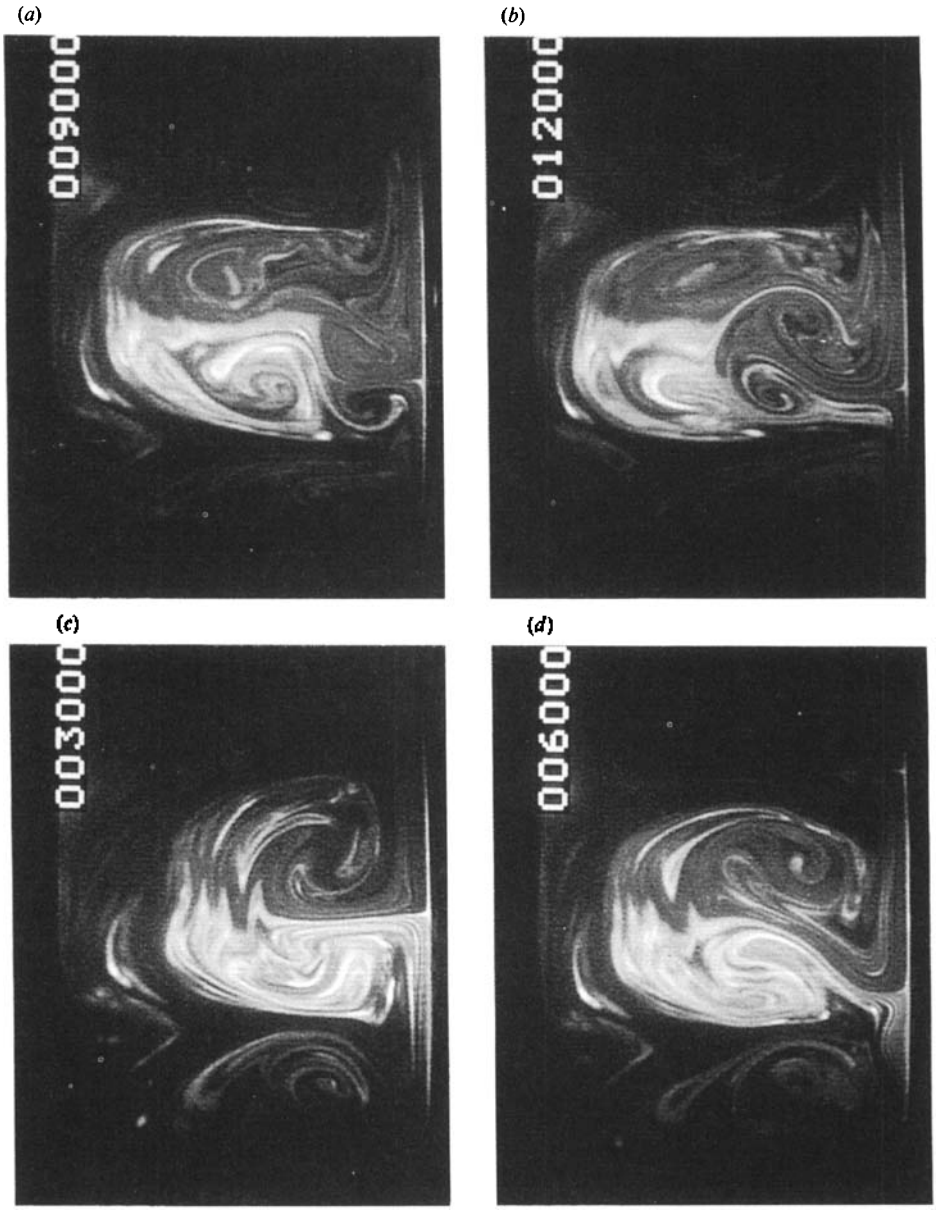

FIGURE 6(*a–d*). For caption see facing page.

bottom of the photograph, close to the inner cylinder, while the largest appears above centre and is elongated across most of the gap. Again, the elongation is primarily due to the outflow boundary of the larger Taylor cells. Similar patterns were observed at higher Taylor numbers.

Flow in a large gap was also examined. Figure 6 shows the development of counter-rotating vortices in a large gap at a Taylor number of 1×10^7; $Ta/Ta_{\text{crit}} = 34.5$. For this large a gap, Taylor cells that spanned the entire gap were never observed over the Taylor number range examined. The photographic sequence shown in figure 6 illustrates the first type of rotational motion observed. The time elapse between successive photographs is 100 s.

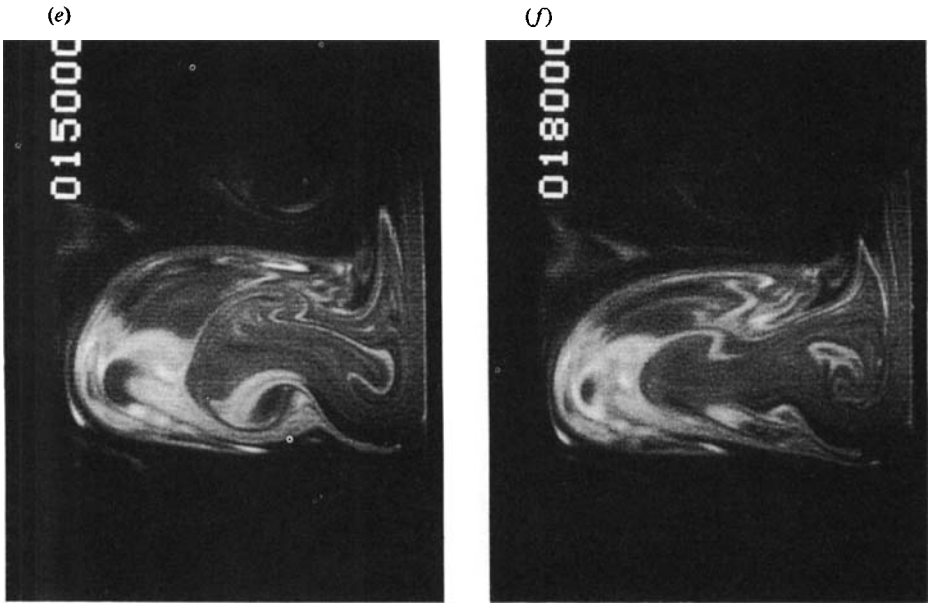

FIGURE 6(*a–f*). Still-photograph sequence made from a large-gap LIF video record at $Ta/Ta_{crit} = 34.5$. The orientation is the same as in figure 4. Time elapse between successive photographs is 100 s.

It is interesting to note here that the Taylor number of this flow is large because of the size of the gap, 13.87 cm. The inner cylinder, the brass shaft, was rotating at only 5.2 revolutions per minute! To obtain the pictures shown in figure 6, the water was placed in the cylinder over 24 hours before the run. Then the inner cylinder was rotated at the appropriate speed for over twelve hours. Dye was placed on the inner cylinder approximately thirty minutes prior to recording the flow on video tape. In addition, the laser was operated only while filming and the laser power was reduced to a minimum to prevent localized heating of the fluid. The salient feature of this sequence is that the rotational motion is very weak. Even when viewed in fast-forward mode, the dye patterns exhibited no circular motion. The flow pattern remains until the formation of a new 'vortex' pair.

At higher Taylor numbers, for the large-gap case, the fluid close to the outer cylinder still did not appear to move very much. However, close to the inner cylinder wall, energetic small-scale counter-rotating vortices were constantly being generated. As the Taylor number is increased, the vortices were generated more frequently. This is shown in figure 7, in which four vortex pairs are clearly visible. This photograph was taken for $Ta/Ta_{crit} = 345$.

The final set of LIF experiments were conducted using a small gap, $d = 1.85$ cm over a Ta range of $20 \leqslant Ta/Ta_{crit} \leqslant 2000$. Representative still photographs taken from video records appear in figure 8. The small gap was the most difficult to obtain publication quality photographs for because of the relatively high speeds involved; the fluorescein dye was rapidly dispersed by the fluid motions. For this reason, the highest Taylor number shown in figure 8 is $Ta/Ta_{crit} = 200$.

Figure 8(*a*) shows a cross-sectional cut of the flow at $Ta/Ta_{crit} = 20$. This is well below the Taylor number at which the counter-rotating vortices first appear. In the video records, the cells appeared to oscillate up and down and their size seemed to oscillate as well. As will

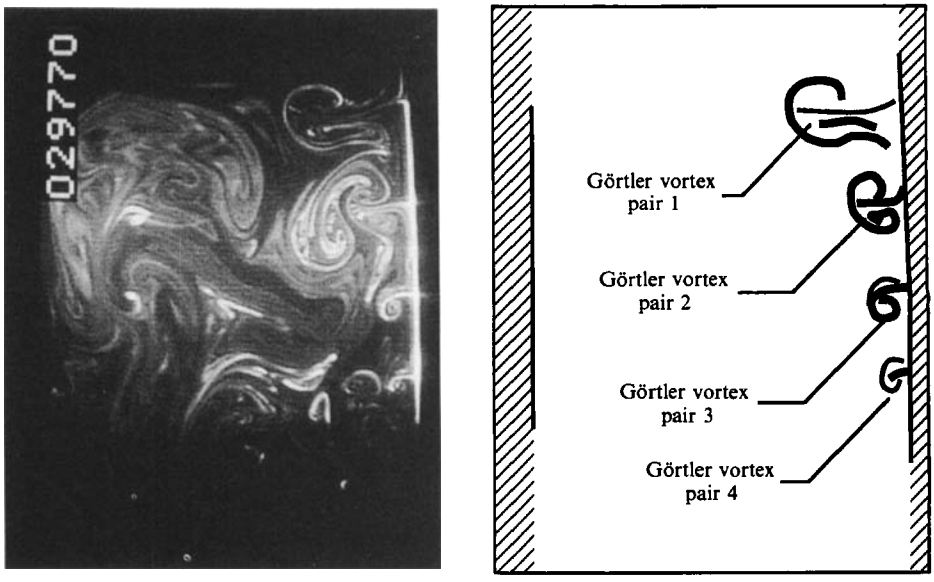

FIGURE 7. Single still photograph and drawing showing simultaneously occurring Görtler vortex pairs at the inner cylinder of a large-gap run. The photograph was taken from a video record at $Ta/Ta_{crit} = 345$. The orientation of the flow is the same as in figure 4.

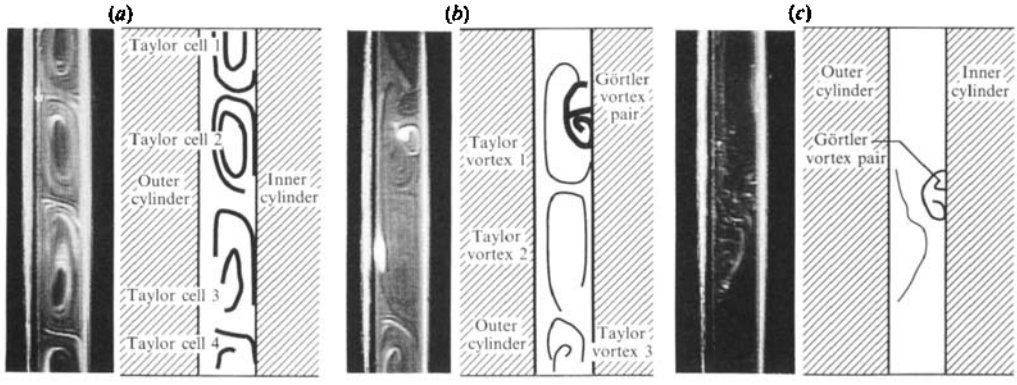

FIGURE 8(*a–c*). Three single still photographs and schematics showing the flow patterns in the small gap at three separate Taylor numbers. The flow orientation is described in figure 4. (*a*) $Ta/Ta_{crit} = 20$; (*b*) $Ta/Ta_{crit} = 67$; (*c*) $Ta/Ta_{crit} = 200$.

be shown in figure 9, this may be attributed to the wavy nature of the Taylor cells at this Taylor number.

In figure 8(*b*), a single photograph is shown for $Ta/Ta_{crit} = 67$. At this Taylor number counter-rotating vortex pairs were observed to form very infrequently at the inner cylinder wall. One such vortex pair appears in the right-hand side of figure 8(*b*). Note that the Taylor cells are still clearly visible.

As the Taylor number is increased, the frequency of occurrence of counter-rotating vortices at the inner cylinder wall increases. Simultaneously, the Taylor cells become less clearly defined in the (r, z)-view LIF experiments. An example of a counter-rotating vortex pair at $Ta/Ta_{crit} = 200$, is presented in figure 8(*c*). A small mushroom shape can be seen at the inner cylinder wall in the centre of the photograph. Notice also that the Taylor cells are not as well defined as in figures 8(*a*)

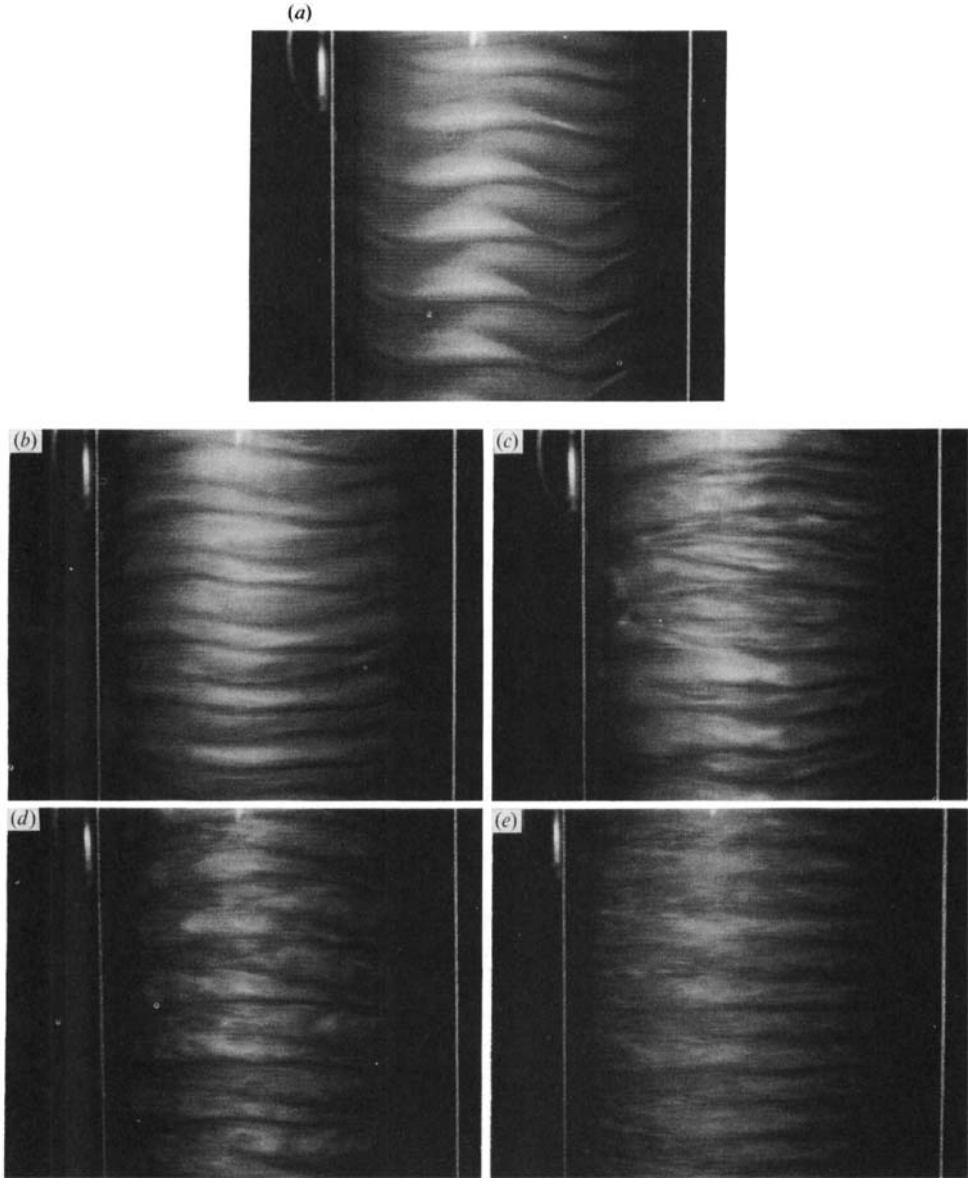

FIGURE 9(*a–d*). Alumina particle visualization photographs of the small-gap flow covering a range of Taylor numbers including that shown in figure 8: (*a*) laminar wavy Taylor vortices at $Ta/Ta_{crit} = 20$; (*b*) wavy vortices at $Ta/Ta_{crit} = 200$; (*c*) the appearance of irregularities in the Taylor vortices, or a 'turbulent spot', at $Ta/Ta_{crit} = 200$ which is caused by Görtler vortex pairs; (*d*) irregular wavy vortices at $Ta/Ta_{crit} = 667$ showing evidence of the 'herringbone' structure; (*e*) turbulent Taylor vortices at $Ta/Ta_{crit} = 2000$ with 'herringbones' similar to that reported by Barcilon *et al.* (1979) and Barcilon & Brindley (1984).

and 8(*b*). As previously stated, the video records made at higher Taylor numbers could not be reproduced well as still photographs.

To connect the LIF experiments with previous visualization experiments, the classic alumina particle flow visualization studies were reproduced as part of this investigation. The resulting photographs are shown in figure 9. In each photograph,

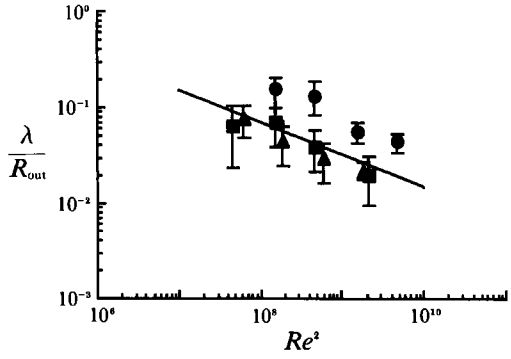

FIGURE 10. Görtler wavelength measurements for the three different gaps plotted using the scaling prescribed by Barcilon & Brindley (1984). The circles, squares, and triangles represent the large, medium, and small gaps respectively. The solid line was obtained from Barcilon & Brindley (1984); it appears in the text as (4).

the cylinder axis of symmetry is oriented vertically. The bright vertical lines are steel cables which were used to hold the top end plate tightly in place, but they correspond to the outer edges of the outer cylinder for this view. In all cases, the inner cylinder is rotating so that the flow is from left to right.

Figure 9(*a*) shows a single still photograph taken at $Ta/Ta_{\text{crit}} = 20$. This is a 0.2 s time-exposure photograph. The wavy nature of the Taylor cells is clearly visible. However, it should also be noted that the Taylor vortices appear to be laminar, albeit wavy, and that in the corresponding LIF experiments, vortex pairs were never observed at the inner cylinder wall.

The photographs comprising figure 9(*b*, *c*) are 0.2 s time exposures taken at $Ta/Ta_{\text{crit}} = 200$ corresponding to the Taylor numbers where counter-rotating vortices infrequently appear (see figure 8*c*). Figure 9(*b*) shows the wavy laminar Taylor cells. Figure 9(*c*) shows the flow at the same Taylor number but with a 'turbulent spot' in the centre. It is argued that this 'spot' is the result of the formation of a counter-rotating vortex pair at the inner cylinder and the resulting disruption of the Taylor cell pattern.

At higher Taylor numbers, the inner-cylinder vortex pairs occur much more frequently. The Taylor cells take on a 'herring-bone' pattern. This is shown in figures 9(*d*) and 9(*e*) for the cases of $Ta/Ta_{\text{crit}} = 667$ and 2000, respectively.

4.2. *Görtler wavelength measurements*

Figure 10 is a plot of Görtler wavelength, non-dimensionalized by the outer-cylinder radius, versus a characteristic Reynolds number squared, $[\Omega R_{\text{out}}{}^2/\nu]^2$, as prescribed by Barcilon & Brindley (1984). Circles, squares, and triangles represent the large-, medium-, and small-gap data, respectively. The error bars in the figures represent 95% confidence intervals computed from the multiple measurements made for each case. It was assumed that the probability density distribution of the data about the mean for each combination of gap width and Taylor number could be represented by a Gaussian with the corresponding mean and standard deviation.

The solid line appearing in the figure was reproduced from the analytical results of Barcilon & Brindley (1984). Using the small-gap approximation and the method of matched asymptotic expansions, they obtained the following relation between Görtler wavelength and their characteristic Reynolds number:

$$\lambda/R_{\text{out}} \propto G_{\text{c}}^{\frac{1}{3}} (\Omega^2 R_{\text{out}}^4/\nu^2)^{-\frac{1}{3}}, \tag{3}$$

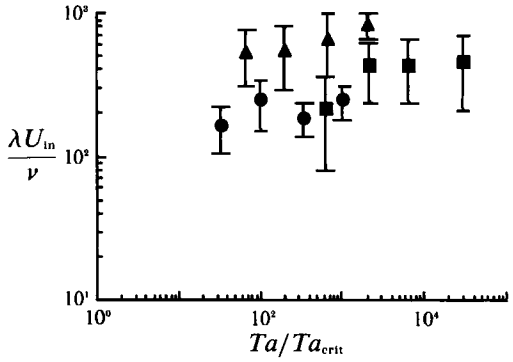

FIGURE 11. Görtler wavelength measurements non-dimensionalized by U_{in} and ν plotted versus Ta/Ta_{crit}. Symbols as in figure 10.

where λ is the Görtler wavelength and G_c is the critical Görtler number for the onset of Görtler vortices. It was not entirely clear how the Görtler number, G, was defined by Barcilon & Brindley (1984); the definition printed in their text was not dimensionless. In their paper, they verified their analysis by plotting unpublished data of Quigley with the following function:

$$\lambda/R_{out} \approx 31.89(\Omega^2 R_{out}^4/\nu^2)^{-\frac{1}{3}}. \tag{4}$$

Observe that (4) is consistent with the form indicated in (3) although, again, it was not clear from their text exactly how Barcilon & Brindley (1984) arrived at the constant of proportionality. The solid line in figure 10 is taken from (4).

It is remarkable how well the present small- and medium-gap data agree with (4). This is construed as additional strong evidence that the vortices shown in §4.1 and the phenomena studied by Barcilon *et al* (1979) and Barcilon & Brindley (1984) are identical. The data follow the $-\frac{1}{3}$ power dependence, which was found by computing a least-squares fit of the data for each gap size. But, even more surprising was that the small- and medium-gap data appear to fall nicely on (4); the intercepts match as well. Because Barcilon & Brindley (1984) used a narrow-gap approximation, it is not surprising that the present large-gap data do not collapse onto (4). This points to the need for an analysis which does not impose the small-gap constraint.

Because the Görtler vortices were observed to form at the inner cylinder wall, it was concluded that the scaling proposed by Barcilon & Brindley (1984) was not sufficiently general to include the large-gap studies. Therefore, three alternative scalings were tried. The characteristic wavelength data non-dimensionalized by the cylinder gap width was plotted as a function of the ratio Ta/Ta_{crit}. The Görtler wavelength was scaled on inner-cylinder radius and plotted versus Ta/Ta_{crit}. Finally, the wavelength data, scaled on inner-cylinder circumferential velocity and the kinematic viscosity of water, were also examined. This last scaling appears to show promise, and is shown in figure 11. However, at this juncture, it is difficult to conclusively identify an appropriate scaling. This issue will be addressed in a separate stability analysis paper by Woodruff & Wei.

5. Discussion

Results of LIF flow visualization experiments of Taylor–Couette flow indicate that at moderately high Taylor numbers, counter-rotating circumferential vortex pairs form close to the inner-cylinder wall. For the small-gap studies, 1.85 cm, these secondary vortices were first observed at Ta/Ta_{crit} between 20 and 50. For the large-

gap case, $d = 13.87$ cm, Taylor vortices were not experimentally observed in this study. Rather, the 'secondary' vortices were the first vortex flow observed.

There are a number of contrasts between the present study and the published works of Barcilon *et al.* (1979) and Barcilon & Brindley (1984). In this study, counter-rotating vortices were observed close to the inner cylinder wall whereas Barcilon and co-workers made their observations primarily at the outer-cylinder wall. (It should be noted, however, that Barcilon & Brindley 1984 comment on unpublished studies in which the 'herring-bone streaks' were observed close to the inner cylinder as well.) In addition, the vortices observed in the present work were first observed at Taylor numbers an order of magnitude lower than those reported by Barcilon *et al.* (1979).

In spite of these differences, the results shown in figure 10 provide strong evidence that the vortices observed close to the inner cylinder wall in the present study and the herring-bone streaks discussed by Barcilon and co-workers are the same phenomenon. The issues to be addressed in the present study, therefore, are: why do the Görtler vortices first appear close to the inner cylinder, and what role do Görtler vortices play in transition to turbulence in Taylor–Couette flows? The first question will be addressed in §5.1 while a discussion of the role of Görtler vortices on the transition to fully turbulent Taylor–Couette flow appears in §5.2.

5.1. *The formation of Görtler vortices at the inner cylinder*

The important parameters governing the strength of the Görtler mechanism are the radius of curvature and the gradient of the velocity. That is, the Görtler mechanism will become stronger as the radius of curvature decreases and/or as the velocity gradient becomes more negative. Obviously, the radius of curvature of the inner cylinder is less than that of the outer cylinder. In addition, the experiments of Smith & Townsend (1982) indicate that the magnitude of the velocity gradient at the inner cylinder is greater than that at the outer cylinder.

Smith & Townsend (1982) plotted the non-dimensional angular momentum, $Ur/U_{\text{in}}R_{\text{in}}$, as a function of non-dimensionalized radial location, $(r-R_{\text{in}})/(R_{\text{out}}-R_{\text{in}})$. U and r are the local circumferential velocity and radial position, respectively. The local velocity gradient at the cylinder walls may be found by rewriting the expression for the gradient of angular momentum:

$$\partial U/\partial r = \{\partial(Ur)/\partial r - U\}/r. \tag{5}$$

For their highest-speed case, $U_{\text{in}} = 9.8$ m/s (the outer cylinder is stationary), the magnitude of the angular momentum gradient, $|\partial(Ur)/\partial r|$, at the inner cylinder wall is approximately 15% greater than the magnitude of the gradient at the outer cylinder wall. For lower speeds, the deviation is even greater. Keeping in mind that $U \geqslant 0$ and $\partial(Ur)/\partial r \leqslant 0$, it is clear from (5) that $|\partial U/\partial r|$ will be greater at the inner cylinder wall than at the outer cylinder wall.

The combination of the inner cylinder having a smaller radius of curvature and a larger (magnitude) velocity gradient than the outer cylinder indicates that Görtler vortices should form at the inner cylinder wall before appearing at the outer cylinder. This does not contradict the work of Barcilon *et al.* (1979) and Barcilon & Brindley (1984). For the small-gap case, the difference between the radii of curvature of the inner and outer cylinders is not very great. Consequently, the characteristic velocity chosen by Barcilon & Brindley (1984), ΩR_{out}, is also not very different from the surface velocity of the inner cylinder. Thus, their analysis showed very good agreement with the present data as shown in figure 10. In fact, Barcilon & Brindley (1984) noted that Mobbs could see structure at the inner cylinder if very light seeding

particle densities were used, but presumably the experiment could not be well photographed. However, the results of this study point to the need to closely examine the flow at the inner cylinder wall in order to gain insight into the formation of Görtler vortices. In addition, it suggests that generalized theoretical analysis of the problem should include inner-wall effects as well as outer-wall effects.

5.2. *Comments on Görtler vortices and the transition to turbulence in Taylor–Couette flows*

Townsend (1984) addressed the problem of transition to turbulence in the Taylor–Couette experiment. He argued that at moderately high Taylor numbers, the near-wall structure was dominated by Görtler vortices, characteristic of curved boundary layers. He further argued that as the Taylor number was increased still further, the near-wall structure became more like that of a plane turbulent boundary layer. This implies that there is a distinct difference between Görtler vortices and plane turbulent boundary layer structure.

This assumption is in conflict with the turbulent boundary layer work of Blackwelder. In a number of studies, the most noteworthy being by Swearingen & Blackwelder (1987), Blackwelder has presented the argument that the near-wall turbulent structure in a plane two-dimensional boundary layer may be caused by the amplification of Görtler instabilities. In short, he argued that small surface imperfections in any physical experiment have sufficient curvature to generate Görtler vortices; near-wall streamwise vortices found in plane turbulent boundary layers are created by the Görtler mechanism. Clearly this contradicts Townsend's (1984) distinction between curvature-generated vortices and plane turbulent boundary layer vortices.

This discrepancy highlights the need for further examination of the turbulence transition processes. Apropos of the Taylor–Couette experiment, it raises the question of the role of Görtler vortices in the transition to turbulence. If Blackwelder's theory is correct, then the Görtler vortices observed in this study are directly contributing to the transition process. As the Taylor number is increased, the Görtler vortices become stronger and more numerous which leads to greater mixing close to the walls. It should be noted, in conclusion, that the Taylor–Couette flow at high Taylor numbers is extremely complex. There are additional structures, such as the flow associated with the inflow and outflow jets, which have not been addressed here.

6. Conclusions

Taylor–Couette flow at moderately high Taylor numbers was examined with LIF flow visualization techniques. The objectives were to test the Barcilon *et al.* (1979) and Barcilon & Brindley (1984) hypothesis that Görtler vortices are generated close to the cylinder wall for $Ta/Ta_{\text{crit}} > 400$, and to gain insight into the role of these vortices in the transition to turbulence in Taylor–Couette flows. A large range of gap sizes and Taylor numbers were examined. Visual observations and measurements of the characteristic wavenumbers of the near-wall vortices led to the following conclusions: (i) the hypothesis of Barcilon and co-workers concerning the formation of Görtler-type vortices in the near-wall boundary layers of Taylor–Couette flows is correct; (ii) however, a complete theoretical analysis must include the observation that Görtler vortices first appear close to the inner cylinder wall and at Taylor numbers an order of magnitude lower than that reported by Barcilon and co-workers.

Funding from the National Science Foundation (Grant no. NSF CTS 89-09230) is gratefully acknowledged. S. L. W. was supported by the DARPA University Research Initiative (Grant N00014-86-K0754).

REFERENCES

BARCILON, A. & BRINDLEY, J. 1984 Organized structures in turbulent Taylor–Couette flow. *J. Fluid Mech* **143**, 429.

BARCILON, A., BRINDLEY, J., LESSEN, M. & MOBBS, F. R. 1979 Marginal instability in Taylor–Couette flows at a very high Taylor number. *J. Fluid Mech.* **94**, 453.

BENJAMIN, T. B. & MULLIN, T. 1982 Notes on the multiplicity of flows in the Taylor experiment. *J. Fluid Mech.* **121**, 219.

CLIFFE, K. A. & MULLIN, T. 1985 A numerical and experimental study of anomalous modes in the Taylor experiment. *J. Fluid Mech.* **153**, 243.

COUGHLIN, K. & MARCUS, P. 1992*a* Modulated waves in Taylor–Couette flow. Part 1. Analysis. *J. Fluid Mech.* **234**, 1.

COUGHLIN, K. & MARCUS, P. 1992*b* Modulated waves in Taylor–Couette flow. Part 2. Numerical simulation. *J. Fluid Mech.* **234**, 19.

FASEL, H. & BOOZ, O. 1984 Numerical investigation of supercritical Taylor-vortex flow for a wide gap. *J. Fluid Mech.* **138**, 21.

FENSTERMACHER, P. R., SWINNEY, H. L. & GOLLUB, J. P. 1979 Dynamical instabilities and the transition to chaotic Taylor vortex flow. *J. Fluid Mech.* **94**, 103.

FLORYAN, J. M. & SARIC, W. S. 1984 Wavelength selection and growth of Görtler vortices. *AIAA J.* **22**, 1529.

GÖRTLER, H. 1954 On the three-dimensional instability of laminar boundary layers on concave walls. *NACA TM* 1375.

HALL, P. 1982 Taylor–Görtler vortices in fully developed or boundary-layer flows: linear theory. *J. Fluid Mech.* **124**, 475.

HALL, P. 1983 The linear development of Görtler vortices in growing boundary layers. *J. Fluid Mech.* **130**, 41.

IOOS, G. 1986 Secondary bifurcations of Taylor vortices into wavy inflow or outflow boundaries. *J. Fluid Mech.* **173**, 273.

JONES, C. A. 1981 Nonlinear Taylor vortices and their stability. *J. Fluid Mech.* **102**, 249.

LEE, S. H.-K. 1990 The effect of drag reducing polymer additives on Taylor–Couette flows. M.S. thesis, dept. of M&AE, Rutgers University.

SMITH, G. P. & TOWNSEND, A. A. 1982 Turbulent Couette flow between concentric cylinders at large Taylor number. *J. Fluid Mech.* **123**, 187.

SPARROW, E. M., MUNRO, W. D. & JONSSON, V. K. 1964 Instability of the flow between rotating cylinders: the wide gap problem. *J. Fluid Mech.* **20**, 35.

SWEARINGEN, J. D. & BLACKWELDER, R. F. 1987 The growth and breakdown of streamwise vortices in the presence of a wall. *J. Fluid Mech.* **182**, 255.

TAYLOR, G. I. 1923 Stability of a viscous liquid contained between two rotating cylinders. *Phil. Trans. R. Soc. Lond.* A **223**, 289.

TOWNSEND, A. A. 1984 Axisymmetric Couette flow at large Taylor numbers. *J. Fluid Mech.* **144**, 329.

VASTANO, J. & MOSER, R. 1991 Short-time Lyapunov exponent analysis and the transition to chaos in Taylor–Couette flow. *J. Fluid Mech.* **233**, 83.

WALOWIT, J., TSAO, S. & DIPRIMA, R. C. 1964 Stability of flow between arbitrarily spaced concentric cylindrical surfaces including the effect of a radial temperature gradient. *Trans. ASME* E: *J. Appl. Mech.* **31**, 585.